# Small-Signal Modeling of a Controlled Transformer Parallel Regulator as a Multiple Output Converter High Efficient Post-Regulator

Agustin Ferreres, Jose A. Carrasco, Enrique Maset, and Juan B. Ejea

*Abstract*—This paper presents a post-regulator based on the use of a controlled transformer, which adds or subtracts an additional voltage to the output filter of a converter in order to regulate its output voltage. So, their actuation is complementary to that of more known post-regulators, such as the magnetic amplifier (magamp) and synchronous switch post-regulator (SSPR), because the regulation is achieved by controlling the voltage across the filter inductor instead of its charge time. Besides, the post-regulator processes the power in parallel to the one flowing from input to output and only handles a percentage of it. The post-regulation by controlled transformer is suitable of being employed in any isolated PWM power converter and combines a good efficiency and the easiness of design of classical switched power supplies. The work describes the post-regulation strategy for obtaining two outputs independently regulated, and presents a model to obtain the control transfer function and the cross-impedance expressions.

*Index Terms*—Magamp, PWM, SSPR.

## I. INTRODUCTION AND BACKGROUND

TECHNIQUES that regulate the different outputs of a multiple output PWM converter may cause cross-regulation effects between the different outputs or may completely eliminate such effects [1], [2]. Among the post-regulating techniques that eliminate cross-regulation for medium-high output currents the most usual are the magamp and the synchronous switch post-regulators (SSPR) [3]–[5]. Both techniques are well known, the idea is to include an element that acts as a switch in order to control the time during which the output inductor is charging at a constant voltage, equal to the secondary winding voltage minus the output voltage.

The alternative that this paper presents consists in the post-regulation by controlled transformer [6], [7]. The principle employed by this technique is based on the addition or subtraction of an ac voltage in the ac path of the inverter. The practical implementation of such technique is shown in Fig. 1. As it can be seen, an auxiliary transformer is connected between the secondary winding of the main transformer and the rectifier. In order to give the proper volt-second product the auxiliary transformer adds a positive or negative voltage while the filter inductor is charging. So, the post-regulator action is complementary to that of the magamp and SSPR because
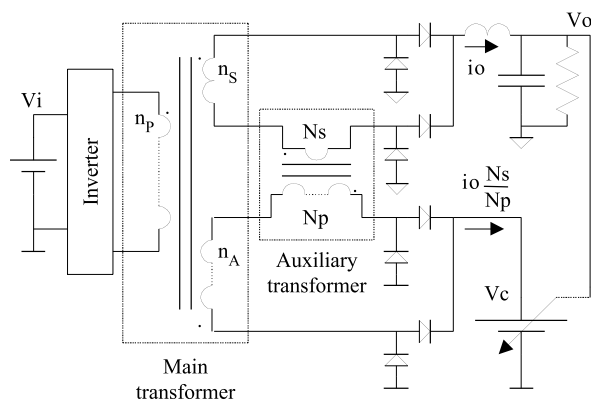
Fig. 1.　Post-regulator circuit with controlled transformer.

the regulation is achieved controlling the voltage across the inductor instead of the charging time.

As Fig. 1 shows, the active element in the regulation process is the controlled voltage source $V_C$, which gives the proper voltage to the primary winding, Np, of the auxiliary transformer. Assuming the inverter output is a square voltage waveform without regulation, the voltage output Vo is

$$V_o = V_i \frac{n_S}{n_P} + \frac{N_S}{N_P} \left\{ V_i \frac{n_A}{n_P} - V_C \right\} \tag{1}$$

and the value that the auxiliary transformer adds

$$\frac{N_S}{N_P} \left\{ V_i \frac{n_A}{n_P} - V_C \right\}. \tag{2}$$

It is clear from (2) that if $V_C$ can take any value between zero and the input voltage, $V_i$, the auxiliary transformer can add a bipolar value between wide ranges; This property permits to obtain the best ratio between its primary winding and secondary winding. In practice, when the main transformer has several secondary windings, it becomes difficult to select the right ratio of the primary winding for each secondary. In these cases, the controlled transformer regulator permits to optimize the main transformer design because with the right choice of $n_A/n_P$ any "effective" main transformer ratio for each output can be simultaneously obtained. In a limit case, should the controlled transformer only add a negative voltage, the auxiliary winding in the secondary side of the main transformer, $n_A$ can be removed and then, as (2) shows, the auxiliary transformer only adds a negative voltage.

Another advantage over classical series post-regulators is that, should the usual conditions design result in $N_S = 1$ the auxiliary transformer only includes a single turn with very low resistance in the path of the output current. It must be also noted that, although the losses in the post-regulator primary side will not be negligible, the total efficiency can be very high due to two reasons. The first one is that, if by a proper design the auxiliary transformer has a ratio $N_P/N_S \gg 1$, the current through the primary side post-regulator will be very small. The second reason is consequence of the mode in which the post-regulator handles the power, it works as a parallel power processor and it only processes a percentage of the total power delivered by the output [8]. This last feature has also an unfavorable effect, which is the main drawback of the post-regulator technique with controlled transformer. The maximum margin of regulation depends on the percentage of power handled by the post-regulator. As a consequence, this technique can be used most effectively when the input voltage variation is limited to a reasonable tolerance range (e.g., $\pm20\%$).

## II. DESIGN CONSIDERATIONS

The design principles must be focused on maximizing the efficiency and the capability of regulation. As explained, the capability of regulation depends on the power handled by the post-regulator but the losses also depend on the handled power. With these premises the current handled by the post-regulator circuitry should be as low as possible in order to minimize losses but the added voltage must be big enough to achieve proper regulation.

From Fig. 1 the most favorable condition to minimize the current in the post-regulator circuitry is a high turns ratio in the auxiliary transformer. Under this design condition the current handled by the post-regulator circuitry is minimized but the voltage that adds the auxiliary transformer decreases when the turns ratio of the auxiliary transformer increases. From (2), the strategy to optimize both, losses and capability of regulation, is to achieve a very wide range variation for $V_C$, in this case the post-regulator can add the proper voltage despite high turns ratio in the auxiliary transformer.

Fig. 1 shows how the voltage source that controls the auxiliary transformer, $V_C$, is a drain for the current from the primary winding of the auxiliary transformer, so power flows toward $V_C$ and basically there are two options to extract the power from $V_C$. The current through the primary side of the auxiliary transformer may be returned to the Vo output, or to the input voltage source. The last option is the best if the voltage output is much lower than the input voltage because, in this case, the auxiliary transformer ratio can be higher [9]. With the premise that the input voltage is much greater than the output voltage, Fig. 2 shows a practical implementation of $V_C$ when the power is returned to the input voltage.

In Fig. 2 implementation the control voltage $V_C$ is the input voltage of an auxiliary converter whose output voltage is $V_i$, the input voltage source. This converter is a boost topology where its input voltage is controlled instead of its output voltage; The output is fixed and equal to $V_i$. Using a PWM control $V_C$ varies
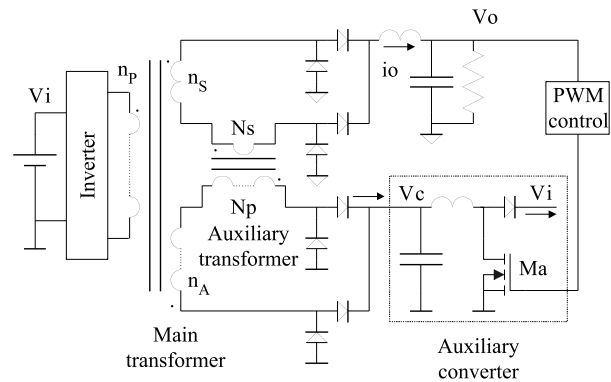


Fig. 2.   Practical implementation of the controlled voltage $V_C$ in which the regulator power is returned to the input.
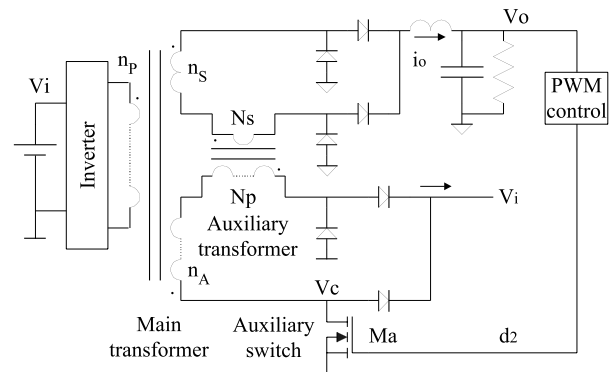


Fig. 3.   Practical implementation of the controlled voltage Vc by an auxiliary switch.

between 0 and $V_i$ when the duty cycle of the switch $M_a$ varies from 100% to near 0%. Thus, the range of $V_C$ is several times greater than that of the output voltage and proper margin of regulation is achieved. From these considerations the post-regulation technique with controlled transformer is particularly suitable for converters with very high output current when the input voltage is much greater than the output voltage.

Another alternative to control the voltage that adds the auxiliary transformer can be seen in Fig. 3 where a new post-regulator circuit is shown. Now a single switch $M_a$ has substituted the auxiliary converter and, if the transformer works in a single quadrant, a rectifier diode also can be eliminated. In the new approach, the value added by the auxiliary transformer depends on the on-off ratio of $M_a$ during each switching period so, $M_a$ has to work synchronized with the inverter switches, preferably in trailing-edge mode to avoid phase-lag [10].

The mean value of the voltage that, according to Fig. 3, adds the auxiliary transformer is

$$V_i \frac{N_S}{N_P} \left\{ \frac{n_A}{n_P} - (1 - d_2) \right\}. \tag{3}$$

The first advantage of this last method of control is evident: the auxiliary converter may be reduced to a single switch. The second one, as this work will show, is a major simplicity of the control loop and the improvement of the dynamic behavior.
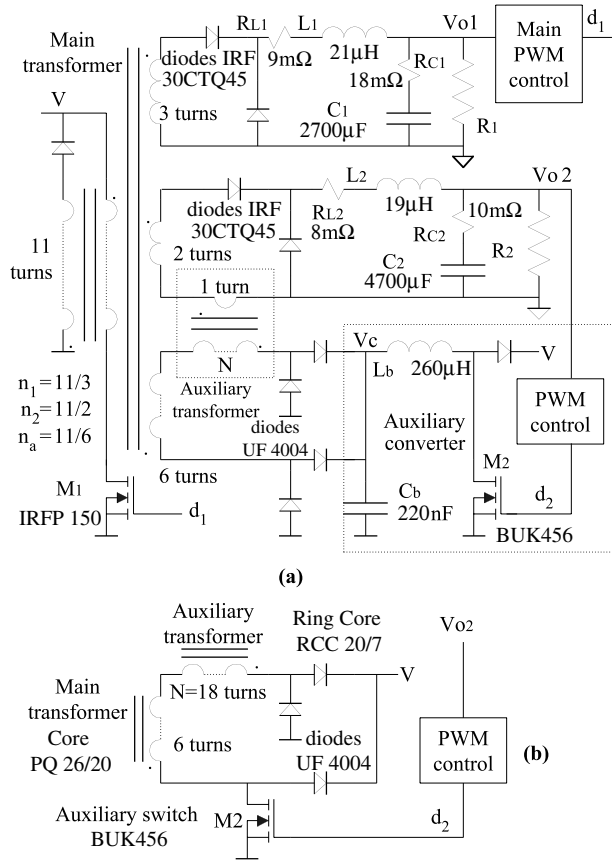
**(a)**



**(b)**

Fig. 4. Experimental prototype developed. (a) Auxiliary transformer controlled by auxiliary converter. (b) Auxiliary transformer circuit controlled by auxiliary switch.

## III. EXPERIMENTAL PROTOTYPE

A 125 W Forward converter with two outputs, 5 V, 15 A, and 3.3 V, 15 A has been build and tested as experimental prototype. The input voltage is 50 V and the switching frequency is 100 kHz.

Both presented circuits to control the voltage that adds the auxiliary transformer have been tested on the experimental prototype. Fig. 4(a) and (b) shows the complete circuit diagram of the converter with both control options.

In both Fig. 4(a) and (b), the main duty cycle, $d_1$, regulates the main output Vo1 (5 V) against changes of line and load, the second output Vo2 (3.3 V) is regulated by a local feedback control loop that adjusts the duty cycle $d_2$. In fact, if the ratio Vo1/Vo2 is equal to ns1/ns2, the main duty cycle already provides proper line regulation to the second output, this condition has been accomplished choosing three turns for the ns1 secondary winding and two turns for ns2 secondary winding. So, since the main duty provides proper line regulation to both outputs the post-regulator will have to add a balanced bipolar voltage to achieve load regulation. From (2) the right choice for the turns ratio of the auxiliary winding is $n_a = 2$, with these conditions the post-regulator is able to add a bipolar voltage that depends of the auxiliary transformer ratio N. The auxiliary transformer ratio has been adjusted to $N = 18$ with a single turn in the secondary side, so the voltage added changes from 0 up to

approximately $\pm(V \div 2N)$ volts in extreme operation condition. A positive value is equivalent to an increment of the duty cycle and a negative value plays the opposite effect. In comparison, the magamp and SSPR always work decreasing the main duty cycle.

In the case of Fig. 4(a), the auxiliary converter may work with any switching frequency; In our case this has been of 100 kHz and with no synchronization to the main switch $M_1$. As known to boost converters, two modes of operation may be possible, the inductor of the auxiliary converter $L_b$, can work in continuous (CCM) or discontinuous conduction mode (DCM) and both modes have been tested to probe its influence on the auxiliary converter dynamics. If $d_1$ is the duty cycle of the main switch $M_1$ and $d_2$ the corresponding to the auxiliary switch $M_2$, the output voltage Vo2 in steady state for the continuous and discontinuous conduction mode are, respectively

$$Vo2 = d_1 V \left( \frac{1}{n_2} + \frac{1}{Nn_a} - \frac{(1-d_2)}{N} \right) \tag{4}$$

$$Vo2 = d_1 V \left( \frac{1}{n_2} + \frac{1}{Nn_a} - \frac{2I_2L_b}{N(2I_2L_b + d_2^2 T_S V_i)} \right) \tag{5}$$

where, in (5), I is the output current and $T_S$ is the switching period. The rest of symbols are shown in Fig. 4(a).

For the case of Fig. 4(b) it must be noted that, as the transformer only adds voltage during the on state of the main switch, the $d_2$ value always will be $d_2 \leq d_1$. The static transfer function of Vo2 in the steady state is

$$Vo2 = d_1 V \left( \frac{1}{n_2} + \frac{1}{Nn_a} - \frac{1}{N} \left( 1 - \frac{d_2}{d_1} \right) \right). \tag{6}$$

## IV. SMALL-SIGNAL MODEL AND DYNAMIC ANALISIS

### A. A Regulation by Auxiliary Converter

Making use of the space-state averaging method [11] the small-signal model of Vo2 is obtained with the auxiliary converter working in continuous conduction mode, and also the main and second outputs working in continuous conduction mode, the usual working strategy for a Forward converter. In order to obtain more compact expressions for the large-signal equations the output filter functions for Vo1 and Vo2 outputs are defined in the Table I

The large-signal equations of the post-regulated output Vo2 can be written as

$$i_{L2} = T_2(s) \left( \frac{Vd_1}{n_2} + \frac{Vd_1}{Nn_a} - \frac{V_C d_1}{N} - Vo2 \right) \tag{7}$$

$$Vo2 = F_2(s) i_{L2}. \tag{8}$$

Assuming CCM in the auxiliary converter the large-signal equations for it are

$$i_{Lb} = \frac{1}{L_b s + R_{Lb}} (V_C - (1-d_2)V) \tag{9}$$

$$V_C = \frac{1}{C_b s} \left( \frac{i_{L2} d_1}{N} - i_{Lb} \right). \tag{10}$$

TABLE I
OUTPUT FILTER FUNCTIONS FOR Vo1 AND Vo2 OUTPUTS

$$F_1(s) = \frac{R_1(Rc_1 C_1 s + 1)}{(Rc_1 + R_1)C_1 s + 1}$$

$$T_1(s) = \frac{1}{L_1 s + R_{L1}}$$

$$F_2(s) = \frac{R_2(R_{C2} C_2 s + 1)}{(R_{C2} + R_2)C_2 s + 1}$$

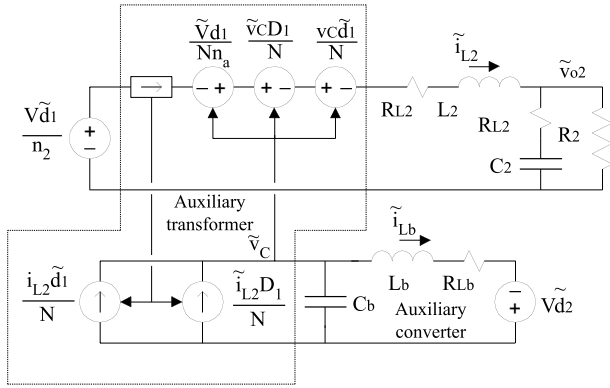$$T_2(s) = \frac{1}{L_2 s + R_{L2}}$$



Fig. 5.   Post-regulated output small-signal circuit.

To obtain more compact expressions the functions $H_1(s)$ and $H_2(s)$ are defined

$$H_1(s) = \left(\frac{1}{L_b s + R_{Lb}} + C_b s\right)^{-1} \tag{11}$$

$$H_2(s) = \frac{V}{L_b s + R_{Lb}}. \tag{12}$$

Now (9) and (10) can be written as

$$V_C = H_1(s)\frac{i_{L2} d_1}{N} + \frac{1}{C_b s(L_b s + R_b) + 1}(V - d_2). \tag{13}$$

The small-signal characteristics of the post-regulated output power stage are derived perturbing the average currents and voltages in (7) to (10) around the DC values (denoted with uppercase letters). The small-signal circuit corresponding to the expressions (7) to (10), particularized to the case in which the input voltage is constant, is shown in Fig. 5. It is clearly visible that the auxiliary transformer acts as a controlled voltage source on the output filter of Vo2 and as a current source that feeds the auxiliary converter.

Next, in order to close the feedback loop we will introduce the dependence of the duty cycle. The new functions involved are $Ae_2(s)$ and $M_2(s)$ corresponding to the compensation and modulator, respectively.
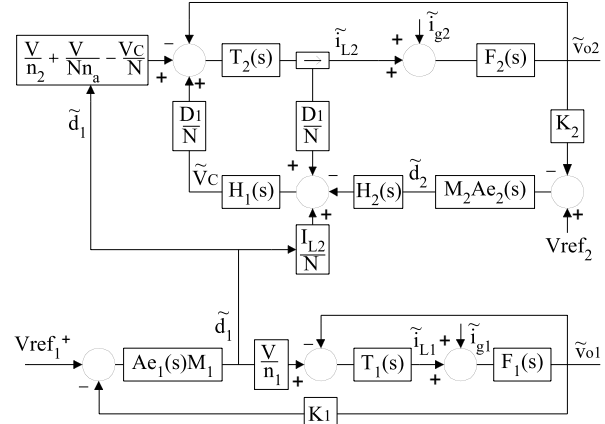


Fig. 6.   Block diagram of the converter small-signal model. Control by an auxiliary boost converter.
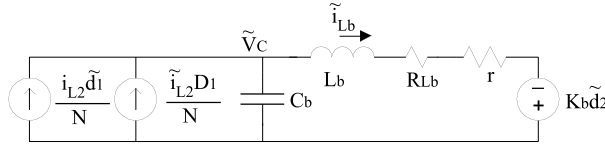


Fig. 7.   Small-signal circuit of the auxiliary converter working in DCM.

Finally, to find the influence of Vo1 over Vo2 the main output Vo1 has been also modeled by the state-space average method [11].

Fig. 6 shows the complete small-signal block diagram of the converter when load perturbations on both outputs, $\tilde{i}_{g1}$ and $\tilde{i}_{g2}$, are introduced.

From Fig. 6 it is clearly visible that the main loop control is independent of the auxiliary loop but the last one depends on the main duty cycle $d_1$. As consequence, the load changes in the main output will affect the second output, therefore the second output has a cross-impedance effect.

The block diagram in Fig. 6 is valid for CCM or DCM in the auxiliary converter but the functions $H_1(s)$ and $H_2(s)$ have to take new expressions if DCM is considered in the auxiliary converter. To considerate this case a new model using the PWM-switch approach has been developed only for the auxiliary converter [12]. The small-signal is shown in Fig. 7, as usual in DCM a dependence on the load appears, the new parameters involved "r" and "$K_b$" are defined in Table II.

Now $H_1(s)$ and $H_2(s)$, will depend of the steady input-output voltages and currents

$$H_1(s) = \left(\frac{1}{L_b s + R_{Lb} + r} + C_b s\right)^{-1} \tag{14}$$

$$H_2(s) = \frac{K_b}{L_b s + R_{Lb} + r}. \tag{15}$$

From (14) and (15) two expected consequences are derived: the loop features have a small dependence on the load magnitude and, as the gain loop Bode diagram will confirm later, the resonance between $C_b$ and $L_b$ is attenuated.

Now, in order to obtain the maximum design easiness, the objective will be to know the open loop transfer function of the Vo2 control loop and to find the explicit form of the cross-impedance

TABLE II
PARAMETERS "r" AND "Kb" AS FUNCTION OF THE STEADY-STATE VALUES

$$D_2 = \sqrt{\frac{(V - V_c)2\,I_2\,L_b}{T_S\,V\,V_c}}$$

$$r = \left( \frac{T_S\,D_2^{\,2}}{2\,L_b} \left( \frac{V_c^{\,2}}{(V - V_c)^2} + \frac{2V_c}{(V - V_c)} + 1 \right) \right)^{-1}$$

$$K_b = \frac{2I_2}{D_2}\,r$$



Fig. 8. Block diagram of the converter small-signal model. Control by an auxiliary switch.

function, $\tilde{V}o2/\tilde{i}_{g1}$, where $\tilde{i}_{g1}$ is the load perturbation on the Vo1 output. From Fig. 6 the open loop control transfer function for Vo2, referred Aol(s), can be easily obtained

$$\text{Aol(s)} = \frac{T_2(s)F_2(s)\frac{D_1}{N}H_1(s)H_2(s)M_2Ae_2(s)K_2}{1 + T_2(s)\left(F_2(s) + \frac{D_1^2}{N^2}H_1(s)\right)}. \quad (16)$$

The first step to calculate the cross-impedance is the evaluation of the influence of main duty changes on the output Vo2. The corresponding transfer function $\tilde{V}o2/\tilde{d}_1$ is (17) shown at the bottom of the page. The transfer function $\hat{d}_1/\tilde{i}_{g1}$ is also obtained from Fig. 6

$$\frac{\tilde{d}_1}{\tilde{i}_{g1}} = \frac{F_1(s)M_1Ae_1K_1}{1 + F_1(s)T_1(s) + F_1(s)T_1(s)M_1Ae_1K_1\frac{V}{n_1}}. \quad (18)$$

From the product of (17) and (18) comes the mathematical expression of closed loop cross-impedance $\tilde{V}o2/\tilde{i}_{g1}$, that is

$$Z_{21} = \frac{\tilde{v}_{o2}}{\tilde{i}_{g1}} = \frac{\tilde{V}o2}{\tilde{d}_1}\frac{\tilde{d}_1}{\tilde{i}_{g1}}. \quad (19)$$

The block diagram in Fig. 6 permits also to calculate the output impedance of Vo2 output, as (20) shows at the bottom of the page.

### B. Regulation by an Auxiliary Switch

Proceeding the same way as before, Fig. 8 shows the block diagram of the small-signal control loop that corresponds to the circuit shown in Fig. 4(b). The new control is simpler than the one on Fig. 6 because the auxiliary switch acts as a controlled
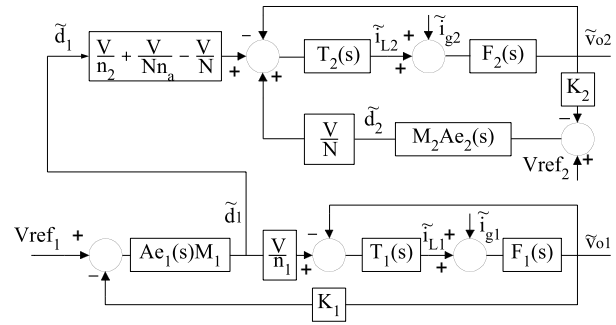
voltage source. It is clearly seen that the parameter N, the turns ratio of the auxiliary transformer, plays as a gain factor in the open loop transfer function.

Now, from Fig. 7, the open loop control transfer function for Vo2, Aol(s), is

$$\text{Aol(s)} = \frac{T_2(s)F_2(s)\frac{V}{N}M_2Ae_2(s)K_2}{1 + T_2(s)F_2(s)}. \quad (21)$$

The transfer function $\tilde{V}o2/\tilde{d}_1$ is presented in

$$\frac{\tilde{v}_{o2}}{\tilde{d}_1} = \frac{\left(\frac{V}{n_1} + \frac{V}{Nn_a} - \frac{V_c}{N}\right)T_2(s)F_2(s)}{1 + T_2(s)F_2(s)\left(\left(1 + \frac{V}{N}M_2Ae_2(s)K_2\right)\right)}. \quad (22)$$

Next, from (17) and (22) and applying (18) the expression of cross-impedance $\tilde{V}o2/\tilde{i}_{g1}$ can be calculated for this situation

$$Z_{21} = \frac{\tilde{v}_{o2}}{\tilde{i}_{g1}} = \frac{\left(\frac{V}{n_2} + \frac{V}{Nn_a} - \frac{V_c}{N}\right)T_2(s)F_2(s)}{1 + T_2(s)F_2(s)\left(\left(1 + \frac{V}{N}M_2Ae_2(s)K_2\right)\right)}$$
$$\times \frac{F_1(s)M_1Ae_1(s)K_1}{1 + T_1(s)F_1(s) + T_1(s)F_1(s)M_1Ae_1(s)K_1\frac{V}{n_1}}. \quad (23)$$

Finally, the expression for Vo2 output impedance is (24), as expected the new expression is simpler than (20)

$$Z_2(s) = \frac{F_2(s)}{1 + T_2(s)F_2(s)\left(1 + \frac{VM_2}{N}Ae_2(s)K_2\right)}. \quad (24)$$

To end the study of cross-impedances we will analyze another cross-impedance function $\hat{V}o1/\hat{i}_{g2}$. Fig. 7 and Fig. 8 show how the second output variables do not affect the main control loop and, as consequence, in voltage control mode, the influence of the second output on the main output may only be possible due

$$\frac{\tilde{v}_{o2}}{\tilde{d}_1} = \frac{\left(\left(\frac{V}{n_1} + \frac{V}{Nn_a} - \frac{V_c}{N}\right) - \frac{I_{L2}D_1}{N^2}H_1(s)\right)T_2(s)F_2(s)}{1 + T_2(s)\left(F_2(s)\left(1 + \frac{D_1}{N}H_1(s)H_2(s)M_2Ae_2(s)K_2\right) + \frac{D_1^2}{N^2}H_1(s)\right)}. \quad (17)$$

$$Z_2(s) = \frac{F_2(s)\left(1 + \frac{D_1^2}{N^2}T_2(s)H_1(s)\right)}{1 + \frac{D_1^2}{N^2}T_2(s)H_1(s) + T_2(s)F_2(s)\left(1 + \frac{D_1}{N}H_2(s)M_2Ae_2(s)K_2\right)}. \quad (20)$$

TABLE III
COMPENSATION TRANSFER FUNCTIONS

| | |
|---|---|
| Case A (CCM) | $Ae_2(s) = \dfrac{6.992(1+s3.9\cdot10^{-4})(1+s2.2\cdot10^{-4})}{(1+s1.287\cdot10^{-5})(1+s1.12\cdot10^{-4})(1+s2.357\cdot10^{-5})}$ |
| Case A (DCM) | $Ae_2(s) = \dfrac{6.992(1+s2.652\cdot10^{-4})(1+s2.16\cdot10^{-4})}{(1+s1.287\cdot10^{-5})(1+s7.41\cdot10^{-5})(1+s1.137\cdot10^{-5})}$ |
| Case B | $Ae_2(s) = \dfrac{8.156(1+s2.652\cdot10^{-4})(1+s2.16\cdot10^{-4})}{(1+s3.96\cdot10^{-5})(1+s7.41\cdot10^{-5})(1+s1.137\cdot10^{-5})}$ |
| Main output | $Ae_1(s) = \dfrac{1.9(1+s3.808\cdot10^{-4})(1+s2.25\cdot10^{-4})}{(1+s3.96\cdot10^{-5})(1+s1.088\cdot10^{-4})(1+s1.406\cdot10^{-5})}$ |



Fig. 9.   Case A with the auxiliary converter in (CCM). Calculated open loop frequency response for the Vo2 output, Aol(s).



Fig. 10.   Case A with the auxiliary converter in (CCM). Measured open loop frequency response for the Vo2 output, Aol(s).



Fig. 11.   Case A with the auxiliary converter in (DCM). Calculated open loop frequency response for the Vo2 output, Aol(s).
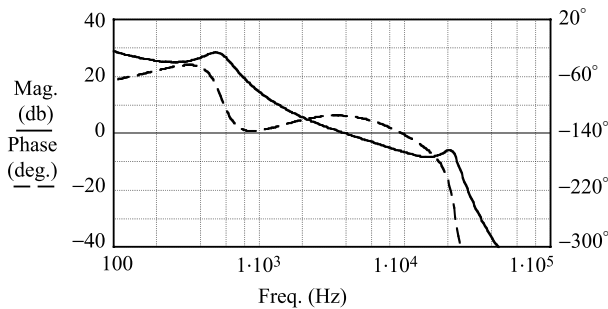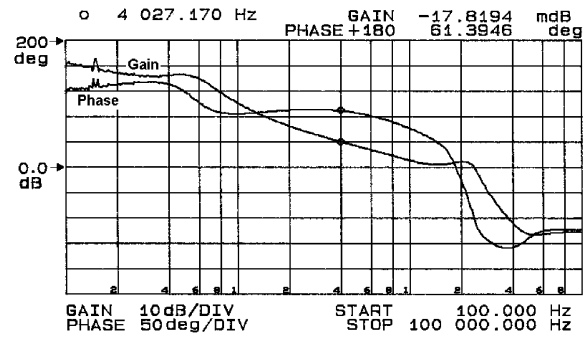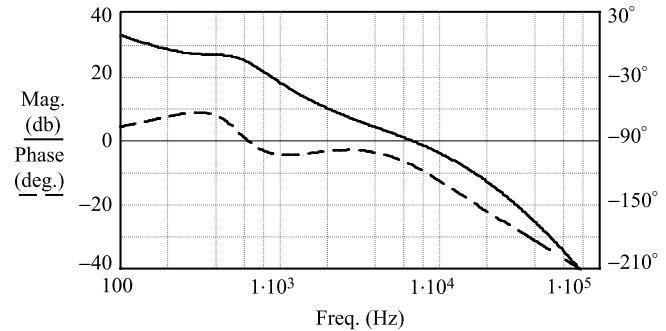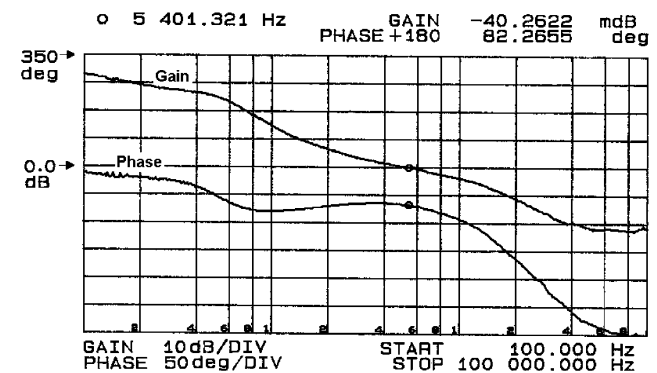


Fig. 12.   Case A with the auxiliary converter in (DCM). Measured open loop frequency response for the Vo2 output, Aol(s).

to parasitic elements of the main transformer. In the next section it will be shown that this interaction is negligible. As a last comment, the line regulation in the second output is better than that of the main output because the main duty already maintains a constant balance volts-second on the secondary Vo2 output.

## V. CALCULATIONS AND MEASUREMENTS

The conditions for all measurements are: nominal input voltage, continuous conduction mode and half load for both outputs. Two main cases will be considered: case A, corresponding to Fig. 4(a) where the auxiliary converter works in CCM or DCM, and case B, corresponding to Fig. 4(b) where the transformer is controlled by the auxiliary switch. To proper comparison between the simulations and the experimental results the compensation functions used can be seen in Table III.

For the case A with the auxiliary converter working in CCM the calculated open loop frequency response for Vo2, Aol(s) corresponding to (16), is shown in Fig. 9.

Note how the resonance between $C_b$ and $L_b$ at 20 kHz affects the gain margin and limits the crossover frequency and the phase margin that can be achieved. The experimental results, in Fig. 10, agree the theoretical measurements.

The calculated and measured open loop transfer function corresponding to (17) when the auxiliary converter works in DCM are shown in Figs. 11 and 12, respectively. Now, it can be seen how DCM increases the damping of the resonance between $C_b$ an $L_b$, this effect would permit an improvement of gain and phase margins. It must be noted that the crossover frequency

has not been increased in order to obtain a proper comparison whit the CCM case.

We would also remark that, as seen in the previous results, better performances can be obtained when the auxiliary converter works in DCM, although the transfer function depends on the current delivered by the output our results have been satisfactory for all the load range.

Now, we analyze case B. The calculated frequency response of the open loop transfer function Aol(s) corresponding to (21) when an auxiliary switch controls the transformer is shown in Fig. 13.

In this case, the crossover frequency and the gain margin are incremented simultaneously because the auxiliary switch does not give any phase lag. The experimental frequency response of (21), in Fig. 14, agrees exactly with the calculated frequency response in Fig. 13.
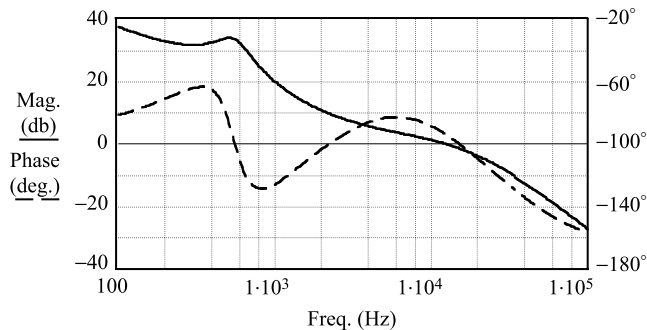
Fig. 13. B case. Calculated open loop frequency response of the Vo2 output, Aol(s).
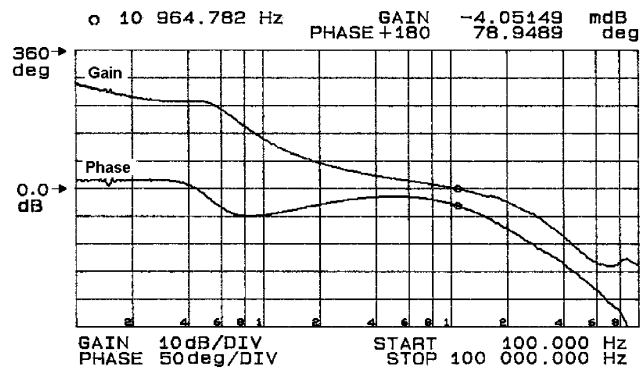


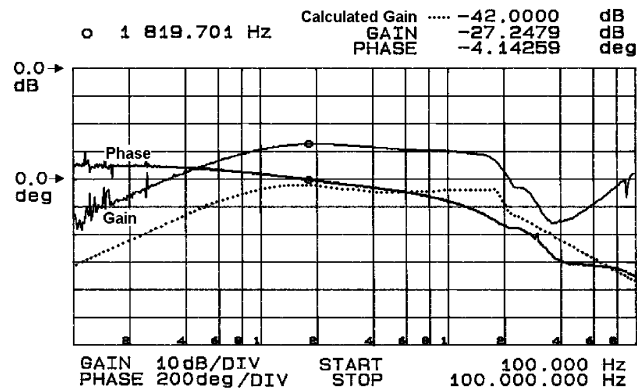Fig. 14. Case B. Measured open loop frequency response for the Vo2 output, Aol(s).



Fig. 15. Case A (CCM). $\check{V}o2/\check{i}_{g1}$ cross-impedance function. Solid lines correspond to measurements and doted lines to predictions. 15 dB shift in gain is due to the measurement setup as explained in text.

Next, we will show the frequency response of the cross-impedance function $\check{V}o2/\check{i}_{g1}$ for cases A and B. The measurements have been made with the electronic load HP 6060A in a gain range of 6 A/V, as consequence, the gain measurement results will have a constant difference of 15 dB with the ones predicted by the model plots. On the other hand, the experimental measurements will be considered valid up to 10 kHz, the bandwidth of the electronic load.

For case A, Figs. 15 and 16 show the cross-impedance function (19) when the auxiliary converter is working in CCM and DCM, respectively. Experimental measurements are solid lines and theoretical prediction doted lines. It can be seen that the experimental measurements agree the calculations of the small-
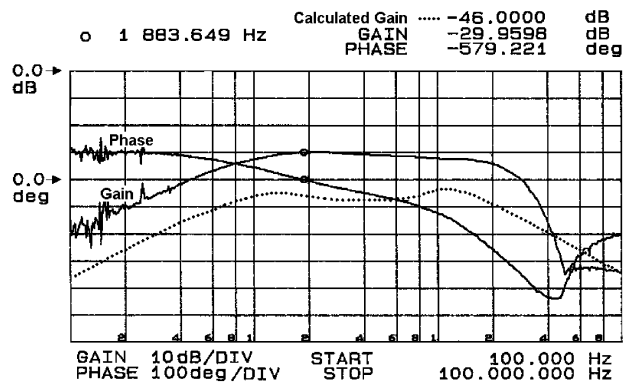


Fig. 16. Case A (DCM). $\bar{V}o2/\bar{i}_{g1}$ cross-impedance function.
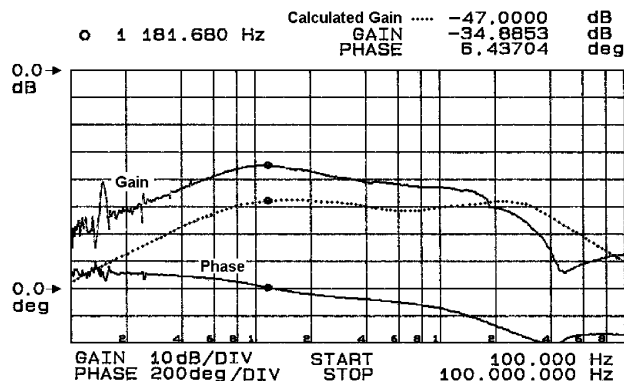


Fig. 17. Case B. $\bar{V}o2/\bar{i}_{g1}$ cross-impedance function.

signal model, taking into account the 15 dB shift due to the measurement setup, and the discrepancies are not significant because they appear above 10 kHz.

Fig. 17 shows the cross-impedance function for the case B corresponding to (23), where the auxiliary switch controls the auxiliary transformer. In this case the loop gain bandwidth, shown in Fig. 14, is bigger what causes a major attenuation in the cross-impedance function.

The influence of the loop gain Aol(s) on the cross-impedance is confirmed in the comparative between Figs. 15–17, they show how successively the cross-impedance function has a major attenuation when the bandwidth of the post-regulator loop gain Aol(s) increases.

The cross-impedance effects in the time domain can be seen in Fig. 18 for the case B. With the auxiliary transformer controlled by the auxiliary switch, a load transient of 2 A on the main output is produced. The magnitude in the transient voltage on the second output expected from the frequency response in Fig. 17.

Finally, Fig. 19 shows the transient voltage in both outputs versus a load transient in the second output, as previously discussed the effect on the main output is negligible over the second one.

## VI. CONCLUSION

The parallel post-regulation method known as controlled transformer has been tested and analyzed in a multiple output PWM converter and the small-signal model in voltage mode control has been obtained for a two outputs case working in
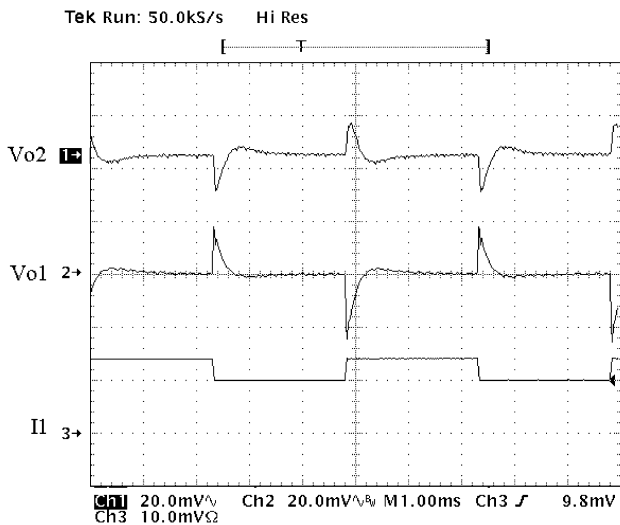
Fig. 18.   Output voltage responses versus load change in Vo1. Scale of $I_1$ 5 A/div.
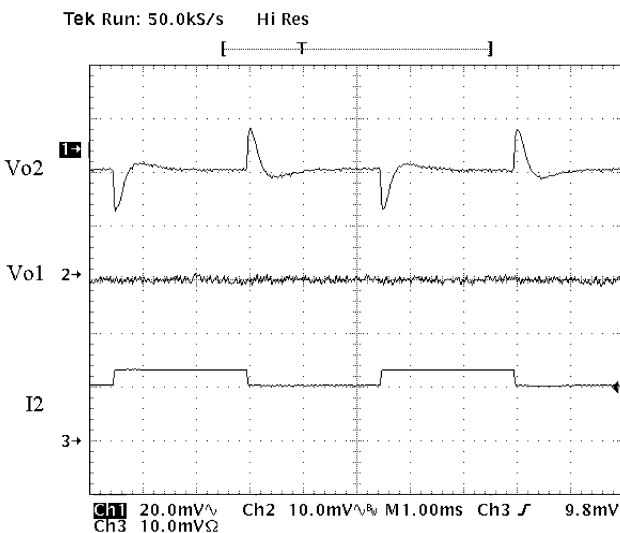


Fig. 19.   Outputs voltage response versus load change in Vo2. Scale of $I_2$ 5 A/div.

continuous conduction mode. The post-regulator by controlled transformer only includes a very low resistance in the path of the output current while the regulation is achieved by handling only a percentage of the power transmitted by the output.

Load changes in the main output produce cross-impedance effects in the post-regulated output whose magnitude decreases when the post-regulator control loop bandwidth increases. Although the auxiliary transformer is equivalent to a gain in the small-signal control loop, the influence of the auxiliary converter, that controls the transformer, has to be considered. In order to achieve a high bandwidth the dynamics of the auxiliary converter should not restrict the crossover frequency of the post-regulator control loop gain. The control of the transformer by the auxiliary switch complies with the above condition and also permits the elimination of the magnetic device of the auxiliary converter. The small-signal model developed has provided the clues to proper design: the open loop transfer function of the post-regulated output and the cross-impedance function.

REFERENCES

[1]  C. L. Jamerson, "Post-regulation techniques for 100 kHz to 300 kHz multiple-output PWM supplies," in *Proc. High Freq. Power Conv. Conf.*, 1989, pp. 260–273.
[2]  Q. Chen, F. C. Lee, and M. M. Jovanovic, "Small-signal analysis and design of weighted voltage control for a multiple-output forward converter," *IEEE Trans. Power Electron*, vol. 10, pp. 589–596, Sept. 1995.
[3]  M. M. Jovanovic and L. Huber, "Small-signal modeling of non ideal magamp PWM switch," *IEEE Trans. Power Electron*, vol. 14, pp. 882–889, Sept. 1999.
[4]  G. Levin, "A new secondary side post-regulator (SSPR) PWM controller for multiple output power supplies," in *Proc. IEEE Appl. Power Electron. Conf.*, 1995, pp. 736–742.
[5]  Y.-T. Chen, "The overall small-signal model of the synchronous switch post-regulator," *IEEE Trans. Power Electron.*, vol. 13, pp. 852–860, Sept. 1998.
[6]  A. H. Weinberg, D. O'Sullivan, and J. A. Carrasco, "Variable transformer turns ratio regulator $\{TR\}^2$ for dc/dc converter or inverter," in *Proc. Eur. Space Power Conf.*, 1993, pp. 33–37.
[7]  Y. G. Kang and A. K. Upadhyay, "A parallel resonant converter with post-regulators," *IEEE Trans. Power Electron*, vol. 7, pp. 296–303, Mar. 1992.
[8]  J. A. Carrasco, A. H. Weinberg, E. Maset, and E. J. Dede, "A high efficiency regulation technique for a zero voltage zero current power switching converter," *IEEE Trans. Power Electron.*, vol. 13, pp. 739–747, July 1998.
[9]  A. Ferreres, J. A. Carrasco, E. Sanchis, J. M. Espí, and E. Maset, "Application of a novel parallel regulation technique in a two output forward converter," in *Proc. IEEE Power Electron. Spec. Conf.*, 1999, pp. 914–919.
[10]  W. Tang, "A new control method for synchronous-switch post regulator," in *Proc. IEEE Power Electron. Spec. Conf.*, 2000, pp. 408–411.
[11]  R. D. Middelbrook and S. Cuk, "A general unified approach to modeling switching-converter power stages," in *Proc. IEEE Power Electron. Spec. Conf.*, 1976, pp. 18–34.
[12]  V. Vorperian, "Simplified analysis of PWM converters using the model of the PWM switch, parts I and II," *IEEE Trans. Aerosp. Electron. Syst.*, vol. 26, pp. 490–505, May 1990.

**Agustin Ferreres** was born in Sant Mateu, Castellón, Spain, on November 26, 1963. He received the M.Sc. degree in physics and the Ph.D. degree in electronics engineering from the Universitat de Valencia, Spain, in 1993 and 1999, respectively.

He worked for a period of two years as a Power Electronics Researcher for the R&D Departmen, GH Industrial. In 1995, he joined the Laboratory of Industrial Electronics and Instrumentation, Universitat de Valencia, Spain. He is now an Associate Professor at the University of Valencia, Spain. His main research areas include space power systems, power supplies, and industrial applications.

**Jose A. Carrasco** was born in Alicante, Spain, in March 1967. He received the M.Sc. degree in physics and the Ph.D. degree in electronics engineering from the Universidad de Valencia, Spain, in 1990 and 1993, respectively.

He worked for a period of two years as a Power Electronics Researcher for the European Space Agency, European Space Research and Technology Center, Noorwijk, the Netherlands. In September 1993, he joined the Laboratory of Industrial Electronics and Instrumentation, Universidad de Valencia, Spain. In 1999, he joined the Universidad Miguel Hernandez where at present he is a Staff Member of the Bioengineering Institute and Leader of the Telemedicine Research Group. He has participated in several projects on power electronics and instrumentation for industrial and space applications and has produced nearly 100 technical papers on these fields. His main research areas include instrumentation, industrial networking, robust control techniques, and high efficiency power conversion.

**Enrique Maset** received the M.Sc. and Ph.D. degrees from the University of Valencia, Spain, in 1988 and 1993, respectively.

He is currently a Professor in the Engineering Electronics Department, Valencia University, where his research interests include power-factor correction techniques and high-frequency and soft-switching conversion techniques for industrial applications.

**Juan B. Ejea** was born in Xátiva, Spain, on June 27, 1969. He received the M.Sc. degree in physics and the Ph.D. degree in electronics engineering from the University of Valencia, Spain, in 1993 and 2000, respectively.

His employment experience include one year in GH Industrial S.A., two years in the Power Section, European Laboratory for Particle Physics, Switzerland, and eight years as an Assistant Professor at the University of Valencia. He is now an Associate Professor at the University of Valencia, Spain, and belongs to the Laboratory of Industrial Electronics and Instrumentation (LEII). His main interests are space power systems and industrial applications.